

Nanoscale

Accepted Manuscript



This is an *Accepted Manuscript*, which has been through the Royal Society of Chemistry peer review process and has been accepted for publication.

Accepted Manuscripts are published online shortly after acceptance, before technical editing, formatting and proof reading. Using this free service, authors can make their results available to the community, in citable form, before we publish the edited article. We will replace this *Accepted Manuscript* with the edited and formatted *Advance Article* as soon as it is available.

You can find more information about *Accepted Manuscripts* in the [Information for Authors](#).

Please note that technical editing may introduce minor changes to the text and/or graphics, which may alter content. The journal's standard [Terms & Conditions](#) and the [Ethical guidelines](#) still apply. In no event shall the Royal Society of Chemistry be held responsible for any errors or omissions in this *Accepted Manuscript* or any consequences arising from the use of any information it contains.

ARTICLE

Cite this: DOI: 10.1039/x0xx00000x

Received 00th January 2012,

Accepted 00th January 2012

DOI: 10.1039/x0xx00000x

www.rsc.org/

Tree Branch-Shaped Cupric Oxide for Highly Effective Photoelectrochemical Water Reduction[†]

Youn Jeong Jang^{a,†}, Ji-Wook Jang^{b,†}, Sun Hee Choi^c, Jae Young Kim^d, Ju Hun Kim^a, Duck Hyun Youn^d, Won Yong Kim^a, Suenghoon Han^a and Jae Sung Lee^{d,*}

Highly efficient tree branch-shaped CuO photocathodes are fabricated by hybrid microwave annealing process with a silicon susceptor within 10 minutes. The unique hierarchical, one-dimensional structure provides more facile charge transport, larger surface areas, and increased crystallinity and crystal ordering with less defects compared to irregular-shaped CuO prepared by conventional thermal annealing. As a result, the photocathode fabricated with the tree branch-shaped CuO produces an unprecedentedly high photocurrent density of -4.4 mAcm^{-2} at 0 V_{RHE} under AM 1.5G simulated sunlight compared to -1.44 mAcm^{-2} observed for a photocathode made by thermal annealing. It is also confirmed that stoichiometric hydrogen and oxygen are produced from photoelectrochemical water splitting on the tree branch-shaped CuO photocathode and a platinum anode.

1. Introduction

Hydrogen production from photoelectrochemical (PEC) water splitting is an attractive way to make solar energy storable, transportable and usable on demand as a fuel. Although water splitting has been intensively investigated since the concept was introduced,¹ still many challenges remain unresolved for practical applications. The requirements on semiconductor photoelectrode materials include a suitable band gap to absorb ample sunlight, appropriate band alignment to split water and good conductivity to extract photogenerated holes and electrons without recombination. Furthermore, for large scale hydrogen production, materials should be inexpensive made of earth-abundant elements and durable in aqueous solutions.

Cupric oxide (CuO) is an attractive cathode material for photoelectrochemical (PEC) water splitting due to its narrow band gap (1.44~1.68 eV) suitable for absorbing a large portion of solar spectrum, of low cost, and nontoxic.² Moreover, it has an appropriate band alignment for water reduction with conduction band edge of -3.66 eV with respect to the vacuum, which is negative enough potential to produce hydrogen from water.³ However, the poor conductivity and the short electron diffusion length (100-200nm) hamper charge transport and separation within semiconductor, increasing the probability of recombination and photo-corrosion. Many approaches have been investigated to overcome this problem of photo-generated charge recombination to enhance photocatalytic or PEC performance such as high crystallinity with a low defect density, large surface area and low dimensional nanoscopic morphology.⁴

Various fabrication methods for CuO have been reported such as spray pyrolysis, metal-organic chemical vapor deposition, and solid state reaction and so on.^{2,5-7} However, these techniques have drawbacks of long fabrication time, low purity CuO phase, many defect sites, and limited product morphology. Here, we report a hybrid microwave annealing (HMA) method to fabricate a unique tree branch-shaped CuO photocathode in a few minutes, which could replace the conventional annealing process. It is well known that microwave induces rapid heating by direct interaction with atoms or molecules of the material, and microwave-assisted synthetic methods have advantages of shortened reaction time and reduced by-product formation. But non-uniform temperature profile between inside and outside of the material is a serious drawback.⁸ The HMA technique combines indirect heating from external heat source called a susceptor and direct heating from microwave. As a result, it is effective for the most materials including non-conducting insulators and provides the temperature uniformity through the material with an extremely short operating time.⁸⁻¹⁰ Thus, in this work, the HMA treatment produced the unique tree branch-shaped CuO with large surface area and reduced defect sites compared to irregularly shaped CuO prepared by conventional thermal annealing. The CuO photocathode of the unique morphology produced an unprecedentedly high cathodic photocurrent of -4.4 mAcm^{-2} under AM 1.5G simulated sunlight at 0 V vs. reversible hydrogen electrode (RHE) in PEC water reduction.

2. Experimental details

2.1 Electrode fabrication

As illustrated in Figure 1, the CuO electrode was fabricated by a two-step process. In the first step, the mixed Cu-Cu oxide (Cu_xO) composite was electrodeposited on the F:SnO₂ (FTO) surface from 0.1 M $\text{Cu}(\text{NO}_3)_2$ (99.9 % Junsei Chemical). The Cu-Cu_xO (denoted as 'Cu FTO') was deposited at an optimized, constant potential of 5 V, which was applied between the two FTO electrodes for 5 min using a DC power supply at room temperature. In the second step, the electrodeposited Cu FTO was oxidized by microwave heating treatment without any susceptor (denoted 'MA Cu_xO'). The tree branch-shaped CuO electrode was obtained from Cu FTO by microwave heating treatment with silicon as a susceptor (denoted as 'HMA CuO') like in Figure S1 (ESI[†]). The home microwave oven provides power of 800 W at 2.45 GHz. The electrodeposited Cu FTO composite was moved onto the silicon wafer (n-type, Silicon Technology Corporation) used as a susceptor, then the microwave reaction proceeded for 10 minutes. The temperature of the synthetic system increased up to almost 400 °C during the HMA treatment. The electrodepositions were carried out at various voltages and the morphologies and photoresponses of final HMA CuO are presented in Figure S2 and S3 (ESI[†]). The 5 V provided the optimum HMA CuO electrode giving the most suitable morphology and the best PEC performance. For comparison, CuO electrode was also fabricated by conventional heating of electrodeposited Cu FTO at 400 °C in a muffle furnace (denoted as 'CAL CuO').

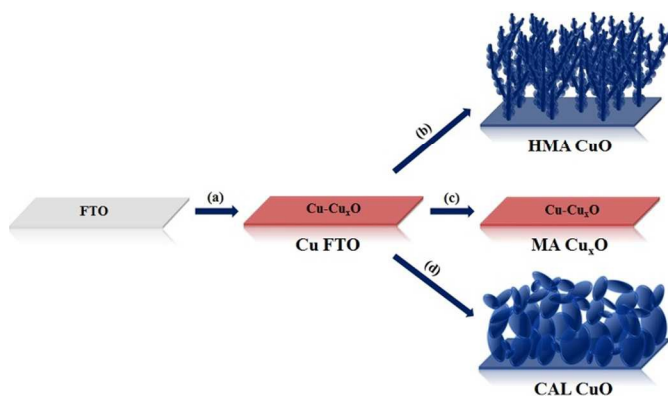


Figure 1. Schematic description of CuO electrode fabrication. (a) Cu-Cu_xO electrodeposited on FTO. (b) Tree branch-shaped CuO fabricated by hybrid microwave annealing (HMA). (c) Cu-Cu_xO by conventional microwave annealing (MA). (d) CuO of an irregular morphology by conventional annealing (CAL).

2.2 Characterization

The morphology of the electrode was characterized by high-resolution scanning electron microscope (HRSEM, JSM-7401F, JEOL) and transmission electron microscopy (TEM, JEM-2200 with image Cs-corrector, JEOL). The crystalline structure and characteristic were analyzed by X-ray diffraction (XRD, PW3040/60 X'pert PRO, PANalytical, with Cu-K α ($\lambda=1.43056\text{\AA}$) radiation). X-ray photoelectron spectroscopy (XPS, ESCALAB 250Xi) measurement was used to confirm surface

state of the electrode. X-ray absorption fine structure (XAFS) measurements were conducted on 7D beamline of Pohang Accelerator Laboratory (PLS-II, 3.0 GeV) in Korea. The radiation was monochromatized using a Si(111) double crystal monochromator. The spectra for the K-edge of Cu ($E_0=8979$ eV) was taken in a fluorescence mode at room temperature. The incident beam was detuned by 20% in order to minimize contamination of higher harmonics and its intensity was monitored using a He-filled IC Spec ionization chamber. The fluorescence signal from the sample was measured under an atmosphere of helium with a PIPS (Passivated Implanted Planar Silicon) detector. ATHENA in the IFEFFIT suite of programs was used to analyze the obtained data for study of the local structure of CuO in the electrode.¹¹

2.3 (Photo)electrochemical measurements

The PEC performance of the electrodes was measured in a 3-electrode system under back-side illumination from a solar simulator (91-160, Oriel) with an air mass 1.5G filter. The simulated light intensity was calibrated to 1 sun (100 mWcm⁻²) using reference guaranteed by National Renewable Energy Laboratories, U.S. The Ag/AgCl electrode in saturated KCl was used as a reference electrode and Pt mesh was used as a counter electrode. The electrolyte was 0.5 M Na₂SO₄ at pH 6. The photo-activity of CuO photocathode was measured under chopped illumination for observing the photo-response under dark and light simultaneously. A potentiostat (IviumStat, Ivium Technologies) applied an external bias potential to the system and the scan rate for the linear sweep voltammetry was 10 mV s⁻¹. The evolved hydrogen and oxygen gases from PEC water splitting were detected by a gas chromatography with TCD (HP 7890, molecular sieve 5 \AA column, Ar carrier gas).

Incident photon to current efficiency (IPCE) was carried out on the same 3-electrode system using 300W Xe lamp (66 905, Oriel Instruments) with monochromator (74-004, Oriel Conerstone 130 1/8 m) with a bandwidth of 5 nm. To prevent $\lambda/2$ radiation originated by Bragg diffraction at the grating, a 299 nm cut-off filter was placed at the exit of the output. Potentiostatic electrochemical impedance spectroscopy (EIS) was carried out at 0 V_{RHE} of DC potential and AC potential frequency range from 100,000 to 0.1 Hz with 10 mV amplitude. The Z-View software (Scribner Associates Inc.) was used to fit obtained data to the corresponding equivalent circuit model. Mott-Schottky (M-S) analysis was measured from 0.5 to 0.9 V_{RHE} DC potential with 10 kHz AC potential frequency and 10 mV amplitude under dark condition.

3. Results and Discussions

3.1 Fabrication and characterization of tree branch-shaped CuO photocathodes

Figure 1 illustrates synthesis strategy of the CuO photoelectrodes. Two FTO glasses are used as a counter electrode and a substrate onto which films of Cu metal and Cu

oxide composite (Cu-Cu_xO) are deposited via electroreduction with a high negative potential (5 V) according to the chemical

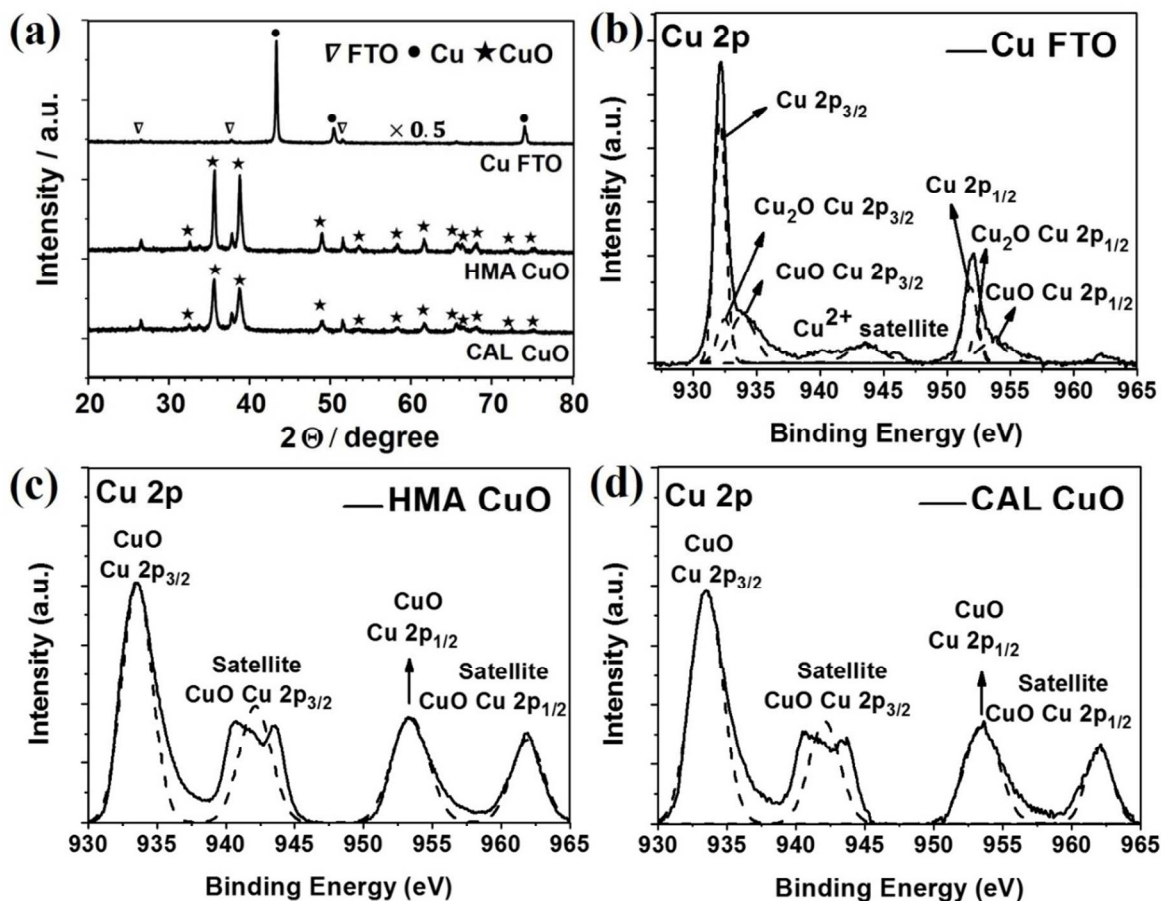
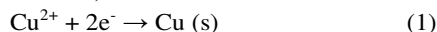


Figure 2. (a) X-ray diffraction (XRD) patterns of electrodeposited Cu-Cu_xO films (Cu FTO), CuO treated with HMA with a silicon susceptor (HMA CuO) and conventional heating at 400 °C (CAL CuO). (b-d) Core-level X-ray photoelectron spectroscopy (XPS) of Cu 2p for Cu FTO (b), HMA (c) and CAL CuO (d).

reaction;¹²



In general, Cu is easily oxidized in water or humid air,¹³ and thus the surface of Cu FTO contained small amounts of Cu₂O and CuO as confirmed by the deconvoluted XPS results for Cu 2p core level in Figure 2b. Doublet peaks located at around 932.3 and 952 eV are attributed to Cu 2p_{3/2} and Cu 2p_{1/2}, respectively, in Cu metal. The peaks shift to 932.5 and 952.3 eV for Cu₂O and 933.7 and 953.6 eV for CuO. However, the XRD pattern of the electrodeposited Cu FTO presents only Cu peaks in Figure 2a, indicating that metallic copper is still the main crystal phase.

Now Cu-Cu_xO in Cu FTO turns to different phases and morphologies upon different annealing processes. Conventional annealing in muffle furnace at 400 °C produced monoclinic phase of CuO (JCPDS no. 01-089-2529) as shown by XRD in Figure. 2a. Below 300 °C, oxidation of Cu was incomplete and Cu and Cu₂O phases were observed as already reported.^{14,15} Conventional microwave annealing (MA Cu_xO) yields mixed phases of Cu (JCPDS no. 01-085-1326) and Cu₂O (JCPDS no. 01-078-2076) as seen by XRD in Figure S4 (ESI[†]). It also shows SnO₂ (JCPDS no. 01-077-0452) contained in FTO

substrate. The temperature of the system during the MA process determined by an IR thermometer laser gun was only 130 °C. As mentioned, this low temperature was not enough to oxidize Cu-Cu₂O to CuO.

For HMA treatment, we first tried graphite as a susceptor. It took only 30 seconds to convert Cu-Cu₂O completely to CuO, but HMA for 20 seconds gave pure Cu₂O (Figure S5). As shown in Figure S6, the system temperature increased over 700 °C with graphite as a susceptor. When silicon was used as a susceptor instead of graphite, the temperature increased to *ca.* 400 °C and longer reaction time (~10 min) was needed to form pure CuO, but control was easier. The XRD pattern of the HMA film with a silicon susceptor shows pure CuO without any Cu or Cu₂O impurities in Figure 2a. By reducing the power of microwave by 80 %, Cu₂O phase can also be obtained (Figure S7). The peak intensity of HMA CuO is much sharper and higher than that of CAL CuO formed at 400 °C, indicating better crystallinity of HMA CuO. The amounts of deposited CuO could also be controlled by regulating the duration in the electrodeposition step. The XPS result of Cu 2p analysis also reveals that single phase CuO is fabricated by HMA treatment in Figure. 2c. In addition to the two peaks at 933.7 and 953.6

eV due to Cu 2p_{3/2} and Cu 2p_{1/2}, the two satellite peaks are observed at around 942 and 962 eV for Cu 2p_{3/2} and Cu 2p_{1/2} from an unfilled 3d⁹ shell of copper.¹⁶

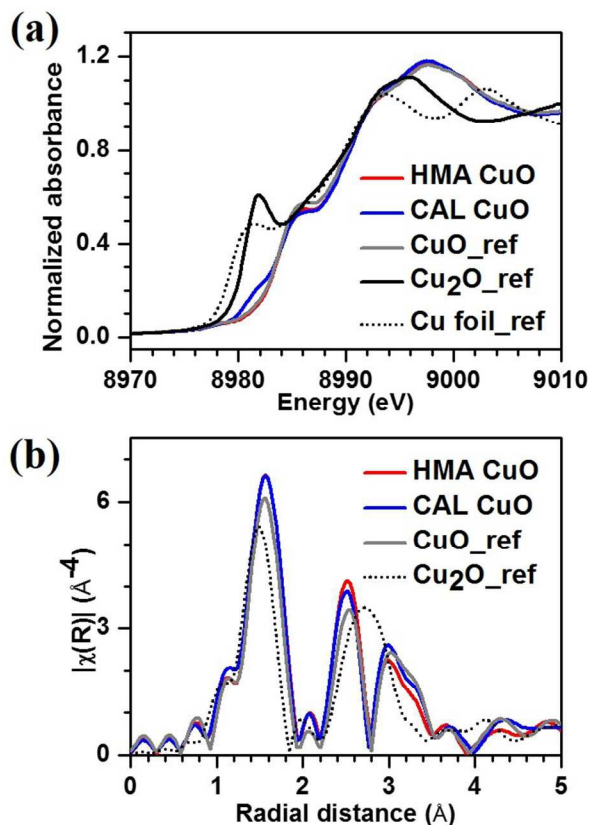


Figure 3. (a) Cu K-edge X-ray absorption near-edge structure (XANES) spectra and (b) k₃-weighted Fourier transforms of Cu K-edge extended x-ray absorption fine structure (EXAFS) functions for electrodeposited CuO films. The spectra for HMA and CAL treatments are compared with those of reference materials CuO, Cu₂O, and Cu foil

X-ray absorption fine structure (XAFS) is an element specific, low concentration-sensitive, and local bulk structure-determining probe. The Cu K-edge X-ray absorption near-edge structure (XANES) in Figure 3a reflects an electric dipole transition from 1s core level to unoccupied p states. Both HMA CuO and CAL CuO sample exhibit similar spectra to reference CuO, but a distinct shoulder is observed at 8979-8984 eV for CAL CuO electrode. Considering that the absorption-rising position is shifted to a lower energy as the oxidation state decreases from +2 to zero, the shoulder could be compared with reference Cu₂O spectrum. The XANES feature of Cu₂O at 8979-8984 eV is matched with the shoulder in terms of energy position. The existence of Cu⁺ in CAL CuO is more clearly visible by their derivative spectra in Figure S8 of ESI†. HMA CuO shows two peaks in 8976-8986 eV; a tiny peak at 8977 eV is due to a quadrupole transition of 1s → 3d observed only for Cu²⁺ materials having unfilled d-orbital (d⁹) and the other intense peak at 8983 eV corresponds to the dipole transition for Cu²⁺ state. However, CAL CuO has three peaks; one tiny peak at 8977 eV, another strong peak at 8981 eV (peak position of

reference Cu₂O) and the other intense peak at 8983 eV. Extended x-ray absorption fine structure (EXAFS) spectra in Figure 3b do not show any significant difference when the samples are compared with reference CuO in powder. Minor difference is increase in the intensities of the peaks at 0.9-2.8 Å. It is due to the enhanced ordering of the nearest Cu-O and Cu-Cu bonds, which is generally observed for the films on substrates. With both XANES and EXAFS results, we come to the conclusion that HMA treatment converts all copper species in the electrodeposited films into CuO phase, but CAL treatment is less effective and impurity Cu₂O is formed within dominant CuO structure.

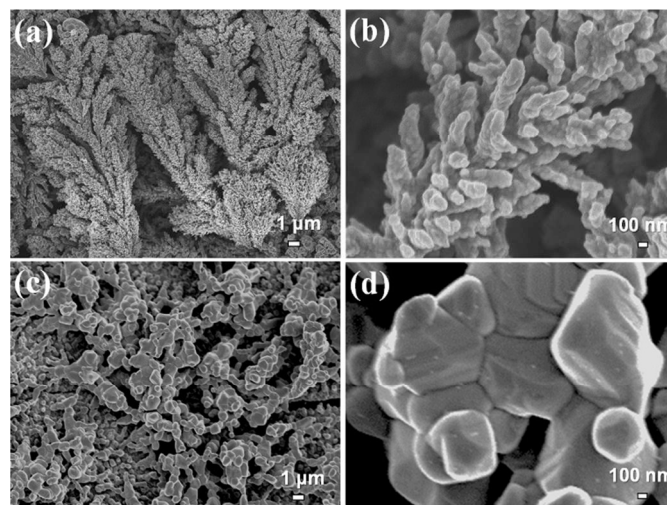


Figure 4. Scanning electron microscopy (SEM) images of tree branch-shape HMA CuO (a and b) and thoes of CAL CuO (c and d)

Morphological characterization was performed by SEM and TEM. Figure 4a,b show the tree branch-shaped CuO electrode treated by HMA with a silicon susceptor. The hierarchical structure is made of nanorods of 100-200 nm in diameter branching continuously away from the substrate like a pine tree. Each nanorod is polycrystalline made of linearly connected nanoparticles of a few 10s of nm. In comparison, CAL CuO electrode fabricated by conventional heating in a muffle furnace, comprises irregular-shaped, aggregated CuO as presented in Figure 4c,d. Both CuO electrodes treated by HMA and conventional calcination are polycrystalline with dominant (111) orientation in Figure S9. The conventional MA treatment without a susceptor could not oxidize Cu-Cu₂O and maintained the initial film morphology of Cu FTO.

Now how does the HMA treatment produce the unique tree leaf-shaped morphology? The susceptor is a good microwave absorber like graphite or silicon and is rapidly heated to a high temperature upon microwave irradiation as in Figure S6 (ESI†). The generated heat is transferred to the target material (Cu-Cu_xO) via the conventional heating mechanism.^{8,17-18} The heated target material can now absorb microwave effectively due to the changed dielectric properties and attenuation distance at the elevated temperature. Thus high and uniform temperature profile is obtained all over the film. At the high temperatures,

Cu and O atoms diffuse rapidly in the material to form copper oxide.^{12,19} This sudden oxidation imposes a large stress on the surface of the electrode due to abrupt increase in the volume during the structural changes.²⁰ One dimensional (1-D) nanostructure formation can minimize the dramatic surface stress among various possible morphologies.¹⁵ Indeed, this extremely fast and high local heating represents the unique feature of the microwave heating including HMA. The better crystallinity of HMA CuO than CAL CuO could also be understood by the higher local temperatures than measured bulk temperatures in the HMA process. This mechanism is consistent with the morphological evolution with HMA duration as presented in Figure S10 (ESI†). In conventional calcination, the speed of Cu diffusion is neither as fast nor as

uniform throughout the Cu electrode and irregular porous morphology is obtained.

In any case, the tree branch shaped HMA CuO presents several desirable properties for efficient PEC devices compared with the CAL CuO fabricated by thermal heating. First, the unique hierarchical 1-D structure could facilitate the rapid charge transport by providing interparticle connection along the nanorod axis as well as nanorod-to-nanorod connection through branches. The facile charge transport is a most essential requirement for any PEC devices. The second is high purity that minimize the defect sites that would trap charge carriers. Finally, it provides high surface areas and pore volumes to secure easy accessibility of electrolyte to the reactive CuO sites.

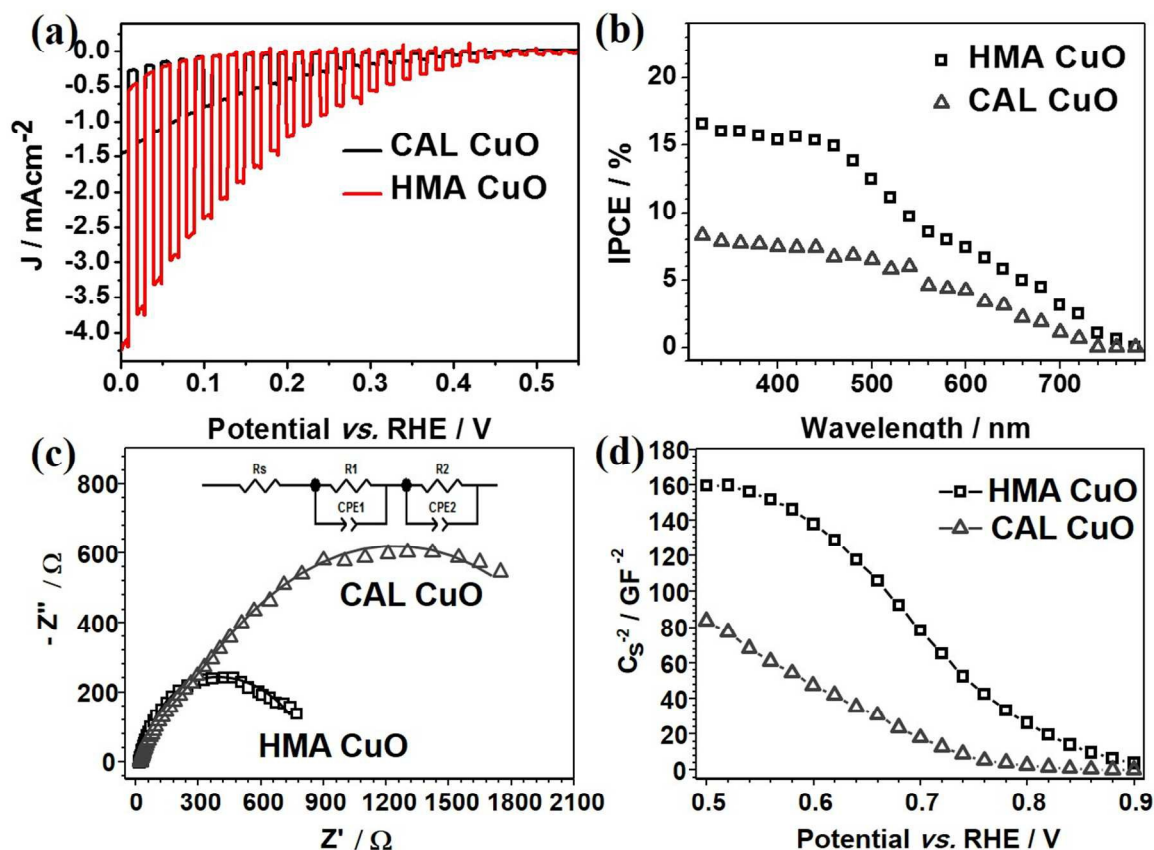


Figure 5. Photoelectrochemical performance of HMA and CAL CuO photocathodes: (a) Photocurrent density (J) and applied potential (V), (b) incident photon to current efficiency (IPCE), (c) potentiostatic electrochemical impedance spectroscopy (EIS) with an equivalent circuit model in the inset, and (d) Mott-Schottky plot

3.2 Photoelectrochemical water reduction

Cupric oxide electrodes were employed as photocathodes for PEC water reduction with a Pt mesh as an anode. The electrodeposited Cu FTO electrode with a composition of $\text{Cu-Cu}_x\text{O}$ has a negligible photo-response as in Figure S11 (ESI†). Figure 5a shows the photocurrent responses of HMA and CAL CuO photocathodes when external bias was applied under irradiation of simulated AM 1.5 G (1 sun) solar light. All the measurements were evaluated under chopped irradiation, so the

dark and light current-voltage could be monitored simultaneously. The photocathodes were scanned only below $0.55 V_{\text{RHE}}$ because the photocurrent showed a plateau above it. At $0 V_{\text{RHE}}$ (the theoretical potential necessary for water reduction), photocurrent of the HMA CuO (-4.4 mAcm^{-2}) was ca. 3 times as high as that of CAL CuO (-1.44 mAcm^{-2}). The HMA CuO photocathode also showed excellent photoresponses under only visible light irradiation ($\lambda > 420 \text{ nm}$) as in Figure S12, and in a highly basic 1 M KOH electrolyte as in Figure S13 of ESI†. Table S1 in ESI† lists the photo-assisted water

reduction activities based on copper oxide photocathodes reported in the literature. There are many unlisted reports that recorded very low photoactivity. It should be mentioned that the photocurrent value observed here records the highest one reported to date for copper oxides photocathodes without co-catalysts for PEC water splitting.

Incident photon to current conversion efficiency (IPCE) was measured for the CuO photocathodes under irradiation with a 300W Xe lamp coupled with a monochromator, and the results are presented in Figure 5b. For both photocathodes, IPCE value starts to increase around the incident light of 700 nm and it is coincident with the known band gap of CuO, ~1.6 eV. Compared with band gap of Cu₂O (2.1 eV), that of CuO (1.6 eV) is much smaller indicating that it can absorb wider solar spectrum. The HMA CuO marks higher IPCE values compared CAL CuO over all wavelengths, indicating that the photogenerated charge transfer and its separation in HMA CuO is better than that of CAL CuO. The relative values of IPCE for HMA and CAL CuO are consistent with the photocurrent results in Figure 5a.

To clarify the origin of the different PEC responses of the HMA and CAL CuO, we performed potentiostatic electrochemical impedance spectroscopy (EIS) measurements. The EIS was measured at -0.6 V vs. Ag/AgCl (0 V_{RHE}) under the light irradiation. The Nyquist plots of CuO photocathodes are presented in Figure 5c. The impedance value of CAL CuO is larger than that of HMA CuO indicating a poor conductivity within the electron pathway in the electrode. For detailed analysis, the EIS data were fitted to a simple equivalent circuit model of two RC circuits as in Figure 5c made of resistance (R) and constant phase element (CPE). Each RC circuit represents an interface between electrode and electrolyte (R2/CPE2) or the electron pathway within the bulk of the electrode (R1/CPE1). The R_s value, the left convergence point of the Nyquist plot, represents sheet resistance in a half cell test system.^{21,22} The fitting results are summarized in Table S2. In general, a large value of resistance in RC circuit takes place at CuO//electrolyte interface (R2/CPE2) because of the large charge transfer resistance and double layer capacitance. The CPE values of HMA CuO as an imperfect capacitor representing surface heterogeneity, roughness and so on are higher compared to CAL CuO.^{23,24} For the HMA CuO photocathode, both of the resistances in the bulk electrode and at the interface of electrolyte and electrode, represented as R1 and R2 respectively, are reduced by 3.7 times.

Mott-Schottky analysis is commonly performed to determine the flat band potential (E_{fb}) of semiconductor as presented in Figure 5d. The tangential line in Mott-Schottky plots is described by:

$$1/C_{sc}^2 = (2/e \epsilon_r \epsilon_0 N) (E - E_{fb} - kT/e) \quad (2)$$

where C_{sc} = space charge layers capacitance, e = electron charge, ε_r = dielectric constant, ε₀ = permittivity of vacuum, N = the charge carrier density, and E = applied potential. Using the equation, E_{fb} and N can be calculated from x-intercepts and

slope in the plots of C_{sc}⁻² vs. applied external potentials. The negative slope indicates that these electrodes show a p-type semiconductor behavior.²⁵ The calculated value of E_{fb} is 0.824 V_{RHE} for HMA CuO and 0.809 V_{RHE} for CAL CuO. There is no significant change in E_{fb} depending on the annealing conditions because both have CuO phase. It is reported that E_{fb} of CuO is higher than that of Cu₂O by around 0.1-0.2 V_{RHE}.^{26,27} The charge density (N) was calculated to be 8.51×10¹⁸ cm⁻³ for HMA CuO, which is less than that of CAL CuO (1.537×10¹⁹ cm⁻³). The higher N value in CAL CuO appears to come mainly from Cu⁺ in the electrode as revealed by XANES in Figure 3. The Cu⁺ sites become centres for charge recombination by trapping photogenerated holes, and thus inhibit charge transfer in CuO instead of promoting it.^{28,29} On the other hands, Cu⁺ defects are removed by further oxidation during the HMA treatment to produce impurity free-CuO phase.

To investigate the stability of the photocathodes under light illumination, the photocurrent was measured under chopped illumination at 0.2 V_{RHE} for 1200 sec in Figure 6a. The HMA CuO electrode shows much higher initial photocurrent in line with the J-V curves in Figure 5a, as well as much better stability than those of CAL CuO. To confirm that H₂ and O₂ are indeed generated from the HMA CuO photocathode and Pt counter electrode during the measurements, the evolving gases were analysed by gas chromatography as shown in Figure 6b. The HMA CuO photocathode was biased at 0.1 V_{RHE} under AM 1.5 light illumination for 60 min. The ratio of produced H₂ and O₂ is close to the stoichiometry and the faradaic efficiencies of oxygen and hydrogen evolution reaction are ca. 88 % and 82 %, respectively. Thus it indicates that the majority of photocurrent observed in the PEC measurements are resulted from photoelectrochemical water splitting reaction. The rest faradaic could be accounted from back reaction of water splitting on working and counter electrode surface and imperfect gas collection due to strong adsorption of evolved gas on the electrode and gas dissolution in the electrolyte.^{30,31} The reduced faradaic efficiency of hydrogen was also considered as slight electron consumption by self-reduction of CuO surface. In spite of those limitations, the gas evolution results clearly show the HMA treated CuO can work effectively for photoelectrochemical overall water splitting. We believe that the stability and faradaic efficiency of CuO can be further enhanced by depositing protective layer.³²⁻³⁴

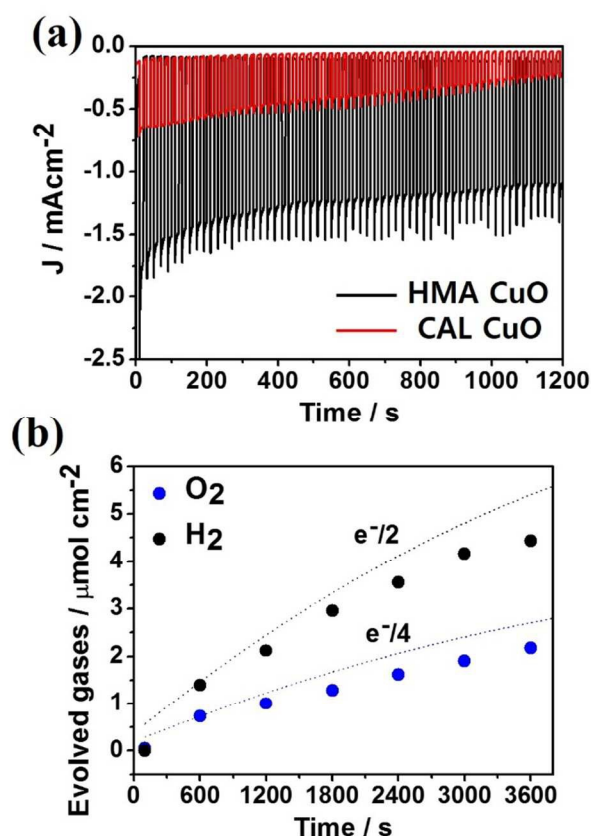


Figure 6. Photoelectrochemical stability tests of HMA and CAL CuO at biased potential of 0.2 V_{RHE} (a) and gas evolution tests (b) from HMA CuO photocathode and Pt anode at biased potential of 0.1 V_{RHE} under 1.5AM simulated 1 sun illumination. The dashed lines indicate expected amounts of evolved oxygen and hydrogen and circles are measured amounts of evolved gases.

4. Conclusions

The HMA process with silicon wafer as a susceptor was introduced for the first time to fabricate a tree branch-shaped CuO cathode for PEC water reduction within a short reaction time of 10 min. The obtained HMA CuO exhibited at least three attributes highly desirable for efficient photoelectrodes distinguished from CAL CuO fabricated by conventional thermal heating: i) The unique hierarchical structure that allows facile charge transport. ii) High crystallinity and purity with less defects that reduces photogenerated charge carrier trap sites and thus carrier recombination. iii) A large surface areas and pore volumes for easy access of electrolyte. As a result, the HMA CuO electrode recorded an excellent photocurrent -4.4 mAcm^{-2} at 0 V_{RHE} , which is the highest value reported to date for copper oxides photocathodes without co-catalyst in PEC water splitting. Work is under progress to improve the PEC activity and stability by a proper surface modification.

Acknowledgements

This work was supported by BK Plus Program (10Z20130011057), Basic Science Research Program (No. 2012-017247), and Korean Center for Artificial Photosynthesis (NRF-2011-C1AAA0001-2011-0030278) funded by the Ministry of Science, ICT and Future Planning of Republic of Korea

Notes and references

^a Department of Chemical Engineering, Pohang University of Science and Technology (POSTECH), San 31 Hyoja-Dong, Pohang, 790-784 South Korea

^b Department of Chemistry, Merkert Chemistry Center, Boston College 2609 Beacon Street, Chestnut Hill, MA, 20467 USA

^c Pohang Accelerator Laboratory, POSTECH, Pohang 790-784 South Korea

^d Department of Energy and Chemical Engineering, Ulsan National Institute of Science and Technology (UNIST), 50 UNIST-gil, Ulsan, 689-798 South Korea. E-mail: jlee1234@unist.ac.kr

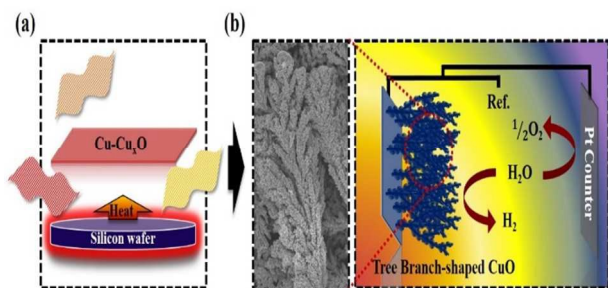
‡ These authors contributed equally to this work.

† Electronic Supplementary Information (ESI) available: The detailed schematic diagram for HMA process, XRD results, the temperature profile during HMA, derivative XANES results, TEM images, J-V curves, lists of previously reported copper oxide photocathode, and parameters extracted from EIS. See DOI: 10.1039/b000000x/

1. A. Fujishima and K. Honda, *Nature*, 1972, **238**, 37-38.
2. C.-Y. Chiang, K. Aroh, N. Franson, V. R. Satsangi, S. Dass and S. Ehrman, *Int. J. Hydrogen Energy*, 2011, **36**, 15519-15526.
3. C.-Y. Chiang, Y. Shin, K. Aroh and S. Ehrman, *Int. J. Hydrogen Energy*, 2012, **37**, 8232-8239.
4. J. Hou, C. Yang, H.-J. Cheng, S. Jiao, O. Takeda and H. Zhu, *Energy Environ. Sci.*, DOI: 10.1039/C4EE02403F.
5. G. G. Condorelli, G. Malandrino and I. L. Fragalà, *Chem. Vap. Deposition*, 1999, **5**, 237-244.
6. W. Jisen, Y. Jinkai, S. Jinquan and B. Ying, *Mater. Des.*, 2004, **25**, 625-629.
7. A. T. Garcia-Esparza, K. Limkraisiri, F. Leroy, S. Rasul, W. Yu, L. Lin and K. Takanebe, *J. Mater. Chem. A*, 2014, **2**, 7389-7401.
8. M. Oghbaei and O. Mirzaee, *J. Alloys Compd.*, 2010, **494**, 175-189.
9. K. H. Brosnan, G. L. Messing and D. K. Agrawal, *J. Am. Ceram. Soc.*, 2003, **86**, 1307-1312.
10. D. H. Youn, J.-W. Jang, J. Y. Kim, J. S. Jang, S. H. Choi and J. S. Lee, *Sci. Rep.*, 2014, **4**.
11. B. Ravel, M. Newville, *J. Synchrotron Radiat.* 2005, **12**, 537-541.
12. P. Wang, Y. H. Ng and R. Amal, *Nanoscale*, 2013, **5**, 2952-2958.
13. I. Platzman, R. Brener, H. Haick and R. Tannenbaum, *J. Phys. Chem. C*, 2008, **112**, 1101-1108.
14. A. Li, H. Song, J. Zhou, X. Chen and S. Liu, *CrystEngComm*, 2013, **15**, 8559-8564.
15. M. Kaur, K. P. Muthe, S. K. Deshpande, S. Choudhury, J. B. Singh, N. Verma, S. K. Gupta and J. V. Yakhmi, *J. Cryst. Growth*, 2006, **289**, 670-675.
16. M. Yin, C.-K. Wu, Y. Lou, C. Burda, J. T. Koberstein, Y. Zhu and S. O'Brien, *J. Am. Chem. Soc.*, 2005, **127**, 9506-9511.
17. W. Shi and N. Chopra, *J. Nanopart. Res.*, 2011, **13**, 851-868.
18. E. Breval, J. P. Cheng, D. K. Agrawal, P. Gigl, M. Dennis, R. Roy and A. J. Papworth, *Mater. Sci. Eng., A*, 2005, **391**, 285-295.
19. J. T. Chen, F. Zhang, J. Wang, G. A. Zhang, B. B. Miao, X. Y. Fan, D. Yan and P. X. Yan, *J. Alloys Compd.*, 2008, **454**, 268-273.

20. A. Kumar, A. K. Srivastava, P. Tiwari and R. V. Nandedkar, *J. Phys.: Condens. Matter*, 2004, **16**, 8531.
21. J. Chen, K. Li, Y. Luo, X. Guo, D. Li, M. Deng, S. Huang and Q. Meng, *Carbon*, 2009, **47**, 2704-2708.
22. L. Han, N. Koide, Y. Chiba, A. Islam, R. Komiyama, N. Fuke, A. Fukui and R. Yamanaka, *Appl. Phys. Lett.*, 2005, **86**, 213501
23. W. H. Mulder, J. H. Sluyters, T. Pajkossy and L. Nyikos, *J. Electroanal. Chem. Interfacial Electrochem.*, 1990, **285**, 103-115.
24. C.-H. Kim, S.-I. Pyun and J.-H. Kim, *Electrochim. Acta*, 2003, **48**, 3455-3463.
25. F. P. Koffyberg and F. A. Benko, *J. Appl. Phys. (Melville, NY, U. S.)*, 1982, **53**, 1173-1177.
26. A. Paracchino, J. C. Brauer, J.-E. Moser, E. Thimsen and M. Graetzel, *J. Phys. Chem. C*, 2012, **116**, 7341-7350.
27. F. Caballero-Briones, J. M. Artés, I. Díez-Pérez, P. Gorostiza and F. Sanz, *J. Phys. Chem. C*, 2008, **113**, 1028-1036.
28. A. Fattah-alhosseini, M. H. Alemi and S. Banaei, *Int. J. Electrochem.*, 2011, 1-6.
29. S. Shen, J. Jiang, P. Guo, C. X. Kronawitter, S. S. Mao, L. Guo, *Nano Energy*, 2012, **1**, 732-741.
30. E. S. Kim, N. Nishimura, G. Magesh, J. Y. Kim, J.-W. Jang, H. Jun, J. Kubota, K. Domen and J. S. Lee, *J. Am. Chem. Soc.*, 2013, **135**, 5375-5383.
31. J. Y. Kim, J.-W. Jang, D. H. Youn, G. Magesh and J. S. Lee, *Adv. Energy Mater.*, DOI: 10.1002/aenm.201400476.
32. Z. Zhang and P. Wang, *J. Mater. Chem.*, 2012, **22**, 2456-2464.
33. B. Seger, T. Pedersen, A. B. Laursen, P. C. K. Vesborg, O. Hansen and I. Chorkendorff, *J. Am. Chem. Soc.*, 2013, **135**, 1057-1064.
34. A. Paracchino, V. Laporte, K. Sivula, M. Grätzel and E. Thimsen, *Nat. Mater.*, 2011, **10**, 456-461.
35. C.-Y. Chiang, J. Epstein, A. Brown, J. N. Munday, J. N. Culver, and S. Ehrman, *Nano Lett.*, 2012, **12**, 6005-6011

Table of Contents Graphic



The tree branch-shaped CuO, fabricated by hybrid microwave annealing (HMA) process with a silicon susceptor shows excellent photoelectrochemical water reduction activity.